International Journal of Mass Spectrometry 447 (2020) 116234

Contents lists available at ScienceDirect

International Journal of Mass Spectrometry

journal homepage: www.elsevier.com/locate/ijms

Full Length Article

Influence of the local environment on the intrinsic structures of gas-phase cytidine-5′-monophosphates

L.A. Hamlow [a], Y.-w. Nei [a], R.R. Wu [a], J. Gao [b], J.D. Steill [b], G. Berden [b], J. Oomens [b], M.T. Rodgers [a, *]

[a] Department of Chemistry, Wayne State University, 5101 Cass Ave, Detroit, MI, 48202, USA
[b] Radboud University, Institute for Molecules and Materials, FELIX Laboratory, Toernooiveld 7c, 6525 ED, Nijmegen, the Netherlands

ARTICLE INFO

Article history:
Received 26 August 2019
Received in revised form
1 October 2019
Accepted 1 October 2019
Available online 15 October 2019

Keywords:
Cytidine-5′-monophosphate
2′-Deoxycytidine-5′-monophosphate
Gas-phase conformation
Infrared multiple photon dissociation (IRMPD) action spectroscopy
Sodium cationization
Mononucleotide

ABSTRACT

Gas-phase conformations of the deprotonated disodium cationized 2′-deoxycytidine-5′-monophosphate and cytidine-5′-monophosphate nucleotides, $[pdCyd-H+2Na]^+$ and $[pCyd-H+2Na]^+$, are studied by infrared multiple photon dissociation (IRMPD) action spectroscopy. Analysis of the experimental results is assisted by complimentary electronic structure calculations of low-energy conformers at the B3LYP/6-311+G(2d,2p)//B3LYP/6-311+G(d,p) level of theory. These calculations provide relative energetics and predicted IR spectra of the calculated conformers for comparison to the measured IRMPD action spectra in the IR fingerprint and hydrogen-stretching regions. Comparisons between the predicted IR and measured IRMPD spectra provide insight into the conformations accessed by $[pdCyd-H+2Na]^+$ and $[pCyd-H+2Na]^+$ during the experiments. Comparison of these calculations and spectroscopic analysis with those performed in previous studies for cytidine nucleotides representing those present in different local environments allows for elucidation of the impact of the local environment on the intrinsic structure of these nucleotides. Comparison of these results with similar studies of the cytidine nucleosides also helps reveal the impact of the phosphate moiety on structure. Although several conformers of both $[pdCyd-H+2Na]^+$ and $[pCyd-H+2Na]^+$ are observed experimentally, a common sodium cation binding mode is observed, highlighting the importance of the stabilization it provides to the cytidine nucleotides.

1. Introduction

Thorough examination of the structural preferences of nucleic acid monomers is important to understanding changes in nucleic acid structure and function in varying environments. Extensive structural studies have been performed on the DNA and RNA nucleic acid monomers in several environments. X-ray crystallography [1–3] and NMR studies [4,5] have been critical in building an understanding of the structures of nucleic acid monomers in the crystalline and solution phase environments in which DNA and RNA structures are most commonly studied [6–10]. However, the complexity and numerous contributors to the intermolecular forces experienced by the molecules in these experiments makes it challenging to isolate the intrinsic structural preferences of the individual monomers. Determining the binding preferences of ions to DNA and RNA is similarly challenged by the complex environments of DNA and RNA, and often relies upon computational models [11–16]. The relatively recent development of gas-phase infrared multiple photon dissociation (IRMPD) action spectroscopy takes advantage of the isolated gas-phase environment and excellent experimental control offered by mass spectrometers to facilitate infrared spectroscopy of specific, isolated ions [17–21]. Complimentary theoretical calculations allow for detailed analysis of the measured IRMPD spectrum and provide insight into the intrinsic gas-phase experimental conformations [22,23].

IRMPD action spectroscopy has been utilized to examine the intrinsic structures of a variety of ionized nucleic acid monomers. The nucleobases of DNA and RNA have been examined by several IRMPD studies to understand the impact of their local environment on structure [24–37]. Binding interactions specific to special

Abbreviations: FELIX, Free Electron Laser for Infrared eXperiments; Cyd, cytidine; dCyd, 2′-deoxycytidine; pCyd, cytidine-5′-monophosphate; pdCyd, 2′-deoxycytidine-5′-monophosphate; FT-ICR MS, Fourier transform ion cyclotron resonance mass spectrometer; QIT MS, quadrupole ion trap mass spectrometer; ESI, electrospray ionization; FEL, free electron laser; OPO, optical parametric oscillator/amplifier; FWHM, full width at half maximum; RMSD, root-mean-square deviation.

* Corresponding author.
E-mail address: mrodgers@chem.wayne.edu (M.T. Rodgers).

https://doi.org/10.1016/j.ijms.2019.116234
1387-3806/

structures such as the i-motif or G-quadruplexes observed in DNA have been examined by IRMPD through several model ion-bound complexes [38–44]. The intrinsic conformations of the common DNA and RNA nucleosides both in their protonated and sodium cationized forms, and several protonated modified nucleosides [45–63] have also been examined in IRMPD action spectroscopy studies. In contrast, IRMPD spectroscopic studies of the DNA and RNA nucleotides have examined the binding of transition metal cations such as Pb^{2+}, Zn^{2+}, and Pt^{2+}, to monophosphate and triphosphate nucleotides, and modified cyclic nucleotides [64–72].

The present work extends our previous studies of the intrinsic structures of the cytidine nucleosides and cytidine-5′-monophosphate nucleotides. The intrinsic gas-phase structures of protonated and sodium cationized 2′-deoxycytidine and cytidine have been thoroughly explored in previous work [45,51,55]. Similar IRMPD studies have also examined the deprotonated [73,74], protonated [75], and sodium cationized forms of the cytidine-5′-monophosphate nucleotides [66]. Representative conformers, typically the computed ground conformers, of these DNA and RNA cytidine-5′-monophosphate nucleotides, are shown in Fig. 1. Deprotonation of the phosphate moiety facilitates binding of two sodium cations to the cytidine-5′-monophosphate anions, resulting in the $[pCyd-H+2Na]^+$ and $[pCyd-H+2Na]^+$ cations. These complexes, which will hereafter be referred to as cytidine nucleotides, present the opportunity to study the importance of different sodium cation binding modes as the limited number of favorable binding sites will limit the nature of the favorable binding modes of one or both sodium cations. Comparison of the cumulative IRMPD studies of the DNA and RNA cytidine nucleosides and nucleotides representing several local environments also allows for examination of the influence of the 2′-hydroxy moiety, the phosphate moiety, and the state of ionization on nucleic acid monomer structure [45,51,66,73,74].

2. Experimental methods

2.1. IRMPD action spectroscopy

The IRMPD action spectra of $[pdCyd-H+2Na]^+$ and $[pCyd-H+2Na]^+$ were acquired in the IR fingerprint region, between 600–1800 cm^{-1}, using a custom-built 4.7 T Fourier-transform ion cyclotron resonance mass spectrometer (FT-ICR MS) coupled to the FELIX free electron laser (FEL, 10 Hz repetition rate, bandwidth 0.3% of the central frequency, energy up to 70 μJ/pulse) [17]. Ions are generated by electrospray ionization (ESI) from solutions of ~1 mM pdCyd or pCyd in 50%:50% methanol:water with ~1 mM NaOH to promote both deprotonation and sodium cationization. pdCyd, NaOH, methanol, and water were purchased from Sigma Aldrich, Zwijndrecht, The Netherlands. The RNA nucleotide, pCyd, was purchased from TCI Europe, Zwijndrecht, Belgium. A detailed description of this FT-ICR MS can be found elsewhere [17]. Ions are generated in a "Z-spray" ESI source and accumulated in a hexapole ion guide. The ions are then injected into the ICR cell through a quadrupole bender and octopole ion guide. Stored waveform inverse Fourier transform (SWIFT) techniques are used in the ICR cell to isolate the ions of interest before they are irradiated by the incident FEL beam in a multi-pass arrangement. Ions are irradiated for 4 s in the IR fingerprint region and 2 s in the hydrogen-stretching region to produce photodissociation, and the resulting ion cloud is mass analyzed and detected. The IRMPD yield is calculated from the precursor ion intensity (I_p) and the fragment ion intensities (I_{f_i}) using Equation (1).

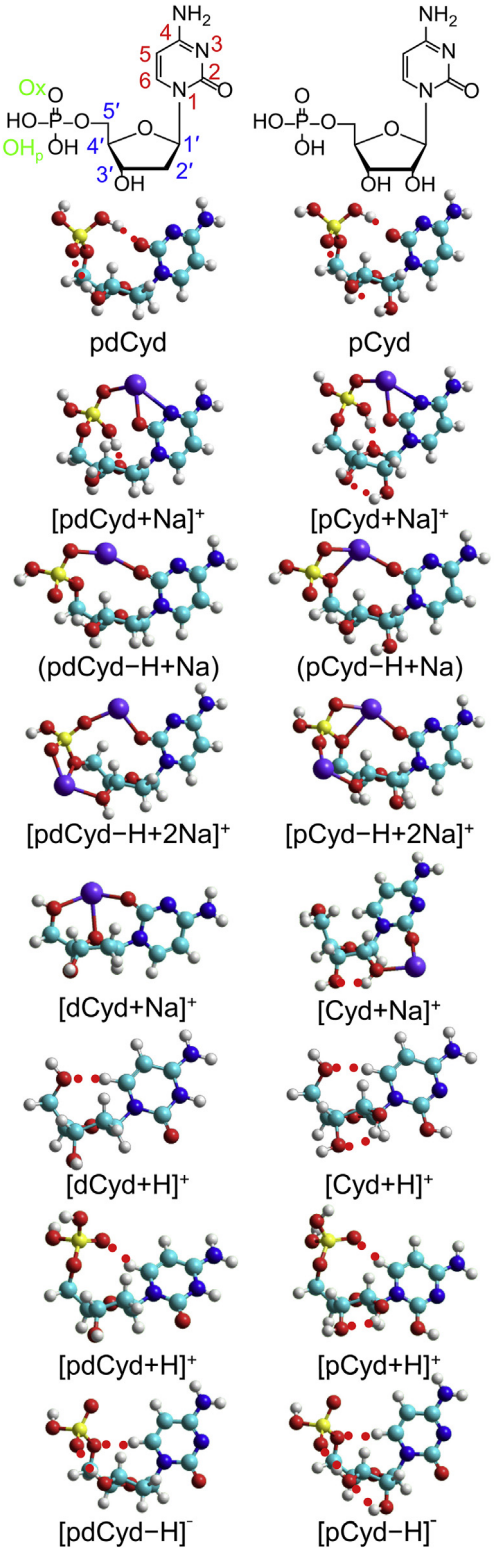

Fig. 1. Chemical structures of 2′-deoxycytidine-5′-monophosphate (pdCyd) and cytidine-5′-monophosphate (pCyd). Low-energy conformers at the B3LYP/6-311+G(2d,2p) level of theory of pdCyd, pCyd, $[pdCyd+Na]^+$, $[pCyd+Na]^+$ [66], (pdCyd−H+Na), (pCyd−H+Na), $[pdCyd-H+2Na]^+$, $[pCyd-H+2Na]^+$, $[dCyd+Na]^+$, $[Cyd+Na]^+$ [51], $[dCyd+H]^+$, $[Cyd+H]^+$ [45], $[pdCyd+H]^+$, $[pCyd+H]^+$ [75], $[pdCyd-H]^-$, and $[pCyd-H]^-$ [73,74]. Atom numbering and labels are provided for the chemical structures and hydrogen-bonding interactions are indicated by red dotted lines. (For interpretation of the references to color in this figure legend, the reader is referred to the Web version of this article).

$$IRMPD\ yield = \sum_i I_{f_i} \Big/ \left(I_p + \sum_i I_{f_i} \right) \quad (1)$$

The IMRPD yield is plotted against the irradiation frequency producing an IRMPD action spectrum.

IRMPD action spectra in the hydrogen-stretching region, 3300−3800 cm^{-1}, were acquired on a modified Bruker amaZon ETD quadrupole ion trap mass spectrometer (QIT MS) [76,77]. Ions were generated by ESI from ~20 μM solutions of pdCyd or pCyd and NaOH in 50%:50% methanol:water. Both pdCyd and pCyd were purchased from Chem Impex, Wood Dale, IL, USA. HPLC grade methanol and water were purchased from Sigma Aldrich, St. Louis, MO, USA. NaOH was purchased from Fisher Scientific, Hampton, NH, USA. Ions were transferred into the quadrupole ion trap, mass isolated, and then irradiated by an optical parametric oscillator/amplifier (OPO) laser (LaserVision, Bellevue, WA, USA, repetition rate 10 Hz, bandwidth 3 cm^{-1}, energy up to 15 mJ/pulse). Precursor and fragment ions were then mass analyzed and detected. The IRMPD yield was calculated using Equation (1) and plotted against the irradiation frequency to produce the measured IRMPD action spectrum.

2.2. Computational methods

To determine the conformers present in the experiments, predicted IR spectra are compared with the measured IMRPD action spectrum. A molecular mechanics conformational search is used to generate high quality candidate structures for this comparison. The starting structures of the two cytidine nucleotide complexes, $[pdCyd-H+2Na]^+$ and $[pCyd-H+2Na]^+$, for this conformational search assumed deprotonation of the phosphate group, and each sodium cation binding to one of the available binding sites. The binding sites examined included both oxo oxygen atoms of the deprtonated phosphate moiety (Ox), the hydroxyl substituents of the phosphate moiety (OH_p), the O2 and N3 atoms of the cytosine nucleobase, and the O4′ and O2′ atoms of the sugar moiety (O2′ is not present in pdCyd), all of which are labeled in Fig. 1. Although not examined experimentally, the neutral ion pairs (pdCyd−H+Na) and (pCyd−H+Na) were also examined by parallel conformational searches and electronic structure calculations for comparison purposes. Each starting structure was submitted to a simulated annealing procedure in HyperChem 8.0 [78] using the Amber 3 force field. Each temperature cycle consisted of 0.3 ps of heating from 0 K to 1000 K, 0.2 ps to sample the accessible conformational space at 1000 K, and 0.3 ps of cooling from 1000 K to 0 K. 3000 temperature cycles were performed for each starting structure with the final structure in each cycle retained as a potential candidate structure. These potential candidate structures were analyzed and the root-mean-square deviation (RMSD) between structures were calculated based on several dihedral angles critical to mononucleotide structure [79]. The five dihedral angles of the sugar ring, ∠C4′O4′C1′C2′, ∠O4′C1′C2′C3′, ∠C1′C2′C3′C4′, ∠C2′C3′C4′O4′, and ∠C3′C4′O4′C1′, the glycosidic bond angle ∠O4′C1′N1C2, the O5′ dihedral angle ∠O4′C4′C5′O5′, and the phosphate dihedral angle ∠C4′C5′O5′P were used to calculate the RMSD between conformers using Equation (2) [57]. X and Y are the sets of dihedral angles measured for the two conformers compared and N is the number of dihedral angles (8).

$$RMSD = \sqrt{\sum_{i=0}^{N} |X_i - Y_i|^2 \Big/ N} \quad (2)$$

An RMSD cut-off was selected based upon manual inspection and chosen to limit the number of conformers examined in greater detail to reduce the cost of the following electronic structure methods. Conformers with RMSD values above that cut-off are identified as unique and submitted to preliminary electronic structure optimizations using density functional theory (DFT) at the B3LYP/6-31+G(d) level of theory in the Gaussian 09 suite [80]. The resulting conformers were then submitted to another RMSD analysis to further refine the selection of unique candidate structures before being subjected to more extensive geometry optimization, frequency analysis, and single point energy calculations at the B3LYP/6-311+G(2d,2p)//B3LYP/6-311+G(d,p) level of theory at 298 K. This level of theory has been found to perform well for similar IRMPD studies of nucleoside and nucleotide ions [45−54,56−58,60−62,75,81−86].

The dihedral angles mentioned above are also used to characterize the specific conformations of the phosphate moiety, sugar ring, and nucleobase. A pseudorotation angle, described in detail elsewhere [79], is calculated from the five sugar dihedral angles and is used to characterize the puckering of the sugar ring. The glycosidic bond angle, O5′ dihedral angle, and phosphate moiety dihedral angle are used to characterize the nucleobase, O5′, and phosphate moiety orientations, respectively. Several distinct sodium binding modes are possible and classified based on the moieties they generally bind together; examples of these binding modes are shown in Fig. 2. Binding of the sodium cation between only the phosphate and nucleobase, in which Ox and O2 are always involved, are classified as α binding, shown as α_1, α_2, α_3, and α_4. In α_3 and α_4, the O_p label is used to specify an oxygen bound to the phosphate, either Ox, OH_p, or O5′. Binding of a sodium cation between the phosphate and sugar moiety through Ox and O4′, with the opportunity to also bind the nucleobase through O2 or the sugar via O5′, is designated as β binding, shown as β_1, β_2, and β_3, with both β_1 and β_2 displaying the additional binding to O2 on the nucleobase, and β_2 and β_3 exhibiting the additional binding to O5′. Binding of a sodium cation to primarily the phosphate moiety, Ox, with the opportunity to bind to the sugar moiety through O3′ and O2′ is designated as the γ binding mode, shown as γ_1, γ_2, and γ_3, with γ_2 additionally binding to the sugar moiety through O3′ and γ_3 binding through O3′ and O2′. The fourth binding mode classified here binds primarily to the nucleobase through O2, and are designated as ε binding modes. ε_1 and ε_2 are shown in Fig. 2 with ε_1 bound between O2 and N3 and ε_2 binding the nucleobase and sugar together through O2 and O2′. To characterize the conformers calculated, each conformer is designated with the two binding modes displayed by the sodium cations. Additionally, the order of relative stability is noted as an alphabetical designation following the two sodium binding mode classifications (with A as the lowest), and the identity of the conformer is given by a subscript 'pdC' or 'pC' to differentiate the DNA and RNA nucleotides for a final conformer designation such as $\alpha_4\beta_2A_{pdC}$.

Vibrational frequencies are predicted during the frequency analysis calculation at the B3LYP/6-311+G(d,p) level of theory. These frequencies are scaled to correct for the anharmonicity present in the real systems, but missing from the harmonic frequencies calculated. This scaling approach is widely used and works reasonably well for similar vibrational modes. Previous work on mononucleotides at this level of theory suggests the need to treat those vibrational frequencies below 1300 cm^{-1}, generally associated with the phosphate moiety differently than those between 1300−1800 cm^{-1} in the IR fingerprint region [65,67,68,72,75,81−83,87,88]. For $[pdCyd-H+2Na]^+$ and $[pCyd-H+2Na]^+$ a scaling factor of 0.9900 was found to work well between 600−1300 cm^{-1}. Slightly greater anharmonicity of modes in the 1300−1800 cm^{-1} range of the IR fingerprint region is

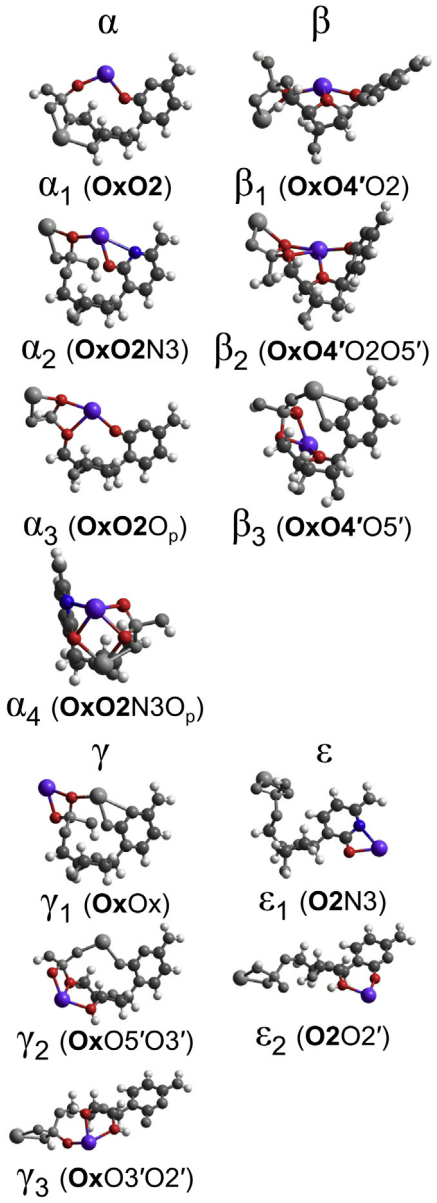

Fig. 2. Four important types of sodium cation binding modes as identified in this work are displayed as α, β, γ, and ε. Specific examples of each binding mode are individually labeled with the specific binding sites of that mode. In the case of α_3 and α_4, O_p indicates any oxygen atom connected to the phosphate. Only the specific sodium binding mode labeled for each conformer is shown in color. (For interpretation of the references to color in this figure legend, the reader is referred to the Web version of this article).

observed for $[pdCyd-H+2Na]^+$ and $[pCyd-H+2Na]^+$ such that scale factors of 0.9780 and 0.9810 perform well. Vibrational modes in the hydrogen-stretching region also require different treatment, as anharmonicity affects them differently than the vibrational modes involving heavier atoms in the IR fingerprint region. A scale factor 0.9610 provides good agreement in the hydrogen-stretching region between 3300–3800 cm^{-1} for both $[pdCyd-H+2Na]^+$ and $[pCyd-H+2Na]^+$. The scaled vibrational frequencies and associated IR intensities are convoluted with 20 cm^{-1} full-width at half-maximum (FWHM) Gaussian peak shapes in the IR fingerprint region and 15 cm^{-1} FWHM in the hydrogen-stretching region to capture the experimental peak widths and facilitate visual comparison of the measured IRMPD and predicted IR spectra.

3. Results

3.1. Theoretical results

3.1.1. $[pdCyd-H+2Na]^+$ and $[pCyd-H+2Na]^+$

Low-energy conformers of $[pdCyd-H+2Na]^+$ and $[pCyd-H+2Na]^+$, shown in Figs. S1 and S2 respectively, display a preference for binding of one sodium cation between the phosphate and nucleobase moieties, α, and the other sodium cation between the phosphate and sugar moieties, β or γ. The structural parameters, sodium binding modes, and relative Gibbs energies for these low-energy conformers are listed in Tables S1 and S2. A comparison of conformers calculated as unique by the RMSD analysis for $[pCyd-H+2Na]^+$ is shown in Fig. S3. Previous studies utilizing a similar conformational search procedure have found much more diverse sugar puckering modes, which are often difficult to differentiate spectroscopically. Therefore, an RMSD cut-off of 30.0° was used for the cytidine nucleotide ions and neutral ion pairs examined in this work. As shown in Fig. S3, an RMSD of 30.0° can differentiate between $\alpha_1\gamma_2B_{pC}$ and $\alpha_1\gamma_1N_{pC}$ which differ in sugar pucker and the rotation of the phosphate moiety resulting in a different binding mode of the second sodium cation. The goal of the RMSD analysis in the conformational searches employed in this work is to identify conformers with unique sodium binding modes in order to produce the largest differences in the predicted IR spectra and reduce the computational cost.

The ground conformers of $[pdCyd-H+2Na]^+$ and $[pCyd-H+2Na]^+$ computed by the conformational search and subsequent DFT calculations display different sodium binding modes. $[pdCyd-H+2Na]^+$ displays a complex $\alpha_4\beta_2$ binding mode with both sodium cations bound relatively close to each other and both interacting with one of the Ox atoms on the phosphate moiety and O2 on the nucleobase. A similar $\alpha_4\beta_2$ conformer is also found for $[pCyd-H+2Na]^+$, but lies 17.2 kJ/mol in Gibbs energy above the calculated $\alpha_3\gamma_2A_{pC}$ ground conformer of $[pCyd-H+2Na]^+$ (shown in Fig. 1). The second most stable conformers calculated for both $[pdCyd-H+2Na]^+$ and $[pCyd-H+2Na]^+$ are nearly identical (shown for $[pdCyd-H+2Na]^+$ in Fig. 1), both with $\alpha_1\gamma_2$ binding, only differing by the O3′H···O2′ intramolecular hydrogen-bonding interaction present in $[pCyd-H+2Na]^+$. Common among the most stable conformers is the binding of at least one sodium cation between the phosphate moiety and nucleobase, with the second sodium cation bound to at least the phosphate moiety. Several conformers were found where the second sodium cation is bound in a γ_1 bidentate binding mode to the Ox and OH_p atoms of the phosphate moiety (see $\alpha_1\gamma_1J_{pdC}$, $\alpha_1\gamma_1N_{pdC}$, $\beta_1\gamma_1I_{pC}$, and $\beta_2\gamma_1J_{pC}$ for examples). Several conformers are also observed with the second sodium cation bound in a γ_1 binding mode to both Ox atoms of the phosphate, such as $\alpha_3\gamma_1E_{pdC}$, $\alpha_2\gamma_1G_{pdC}$, $\alpha_3\gamma_1C_{pC}$, and $\alpha_3\gamma_1F_{pC}$. Binding of one of the sodium cations to the sugar moiety in a β binding mode, with the sodium cation bound between the phosphate moiety and nucleobase moiety through O4′ is also observed in many conformers (see $\alpha_1\gamma_2B_{pdC}$, $\alpha_3\beta_2D_{pdC}$, $\alpha_4\beta_2D_{pC}$, $\alpha_3\beta_3E_{pC}$ for examples). In addition to the Ox and OH_p binding sites on the phosphate moiety, O5′ can also be positioned in such a way as to interact with the sodium cation binding either the phosphate and nucleobase in β_2 binding such as in $\alpha_4\beta_2D_{pC}$, or the phosphate and sugar moiety in γ_2 binding such as $\alpha_1\gamma_2B_{pC}$.

Conformers that do not bind a sodium cation between the phosphate moiety and nucleobase lie much higher in energy, ≥60 kJ/mol for both $[pdCyd-H+2Na]^+$ and $[pCyd-H+2Na]^+$. These conformers generally display bidentate binding modes for both sodium cations, one involving an Ox atom of the phosphate moiety, and the other to the N3 and O2 atoms of the nucleobase. Only a few representative conformers with this binding mode are shown in

Figs. S1 and S2, but the absence of a sodium binding mode simultaneously involving both the phosphate moiety and nucleobase results in a myriad of possible orientations for both of these groups. Some conformers were calculated that did not display sodium cation binding with the nucleobase, but they lie particularly high in Gibbs energy (see $\gamma_3\gamma_1 S_{pC}$ and $\gamma_3\gamma_1 T_{pC}$ for examples).

3.1.2. Neutral (pdCyd−H+Na) and (pCyd−H+Na) ion pairs

Low-energy conformers of neutral (pdCyd−H+Na) and (pCyd−H+Na) ion pairs are shown in Figs. S4 and S5, and structural parameters for these conformers are listed in Tables S3 and S4, respectively. The calculated ground conformers of (pdCyd−H+Na) and (pCyd−H+Na) prefer α sodium binding modes. (pdCyd−H+Na) prefers an α_1 sodium cation binding mode between Ox and O2, whereas (pCyd−H+Na) prefers the α_3 binding mode between Ox, O2, and O5′. Both ground conformers also stabilize the hydroxy moieties of the sugar through hydrogen-bonding interactions with the second Ox atom of the phosphate moiety. Conformers displaying β type binding modes, involving binding of the sodium cation to the phosphate moiety, sugar moiety, and nucleobase, are observed within 15.4 and 29.9 kJ/mol for (pdCyd−H+Na) and (pCyd−H+Na), respectively. Conformers that lack an interaction with the nucleobase are also observed in the calculations, but lie ≥44.0 and 39.6 kJ/mol higher in Gibbs energy for (pdCyd−H+Na) and (pCyd−H+Na), respectively.

3.2. IRMPD spectroscopy results

Photodissociation of $[pdCyd-H+2Na]^+$ primarily leads to N-glycosidic bond cleavage resulting in loss of neutral cytosine. Phosphate ester bond cleavage and water loss results in the observation of $[PO_3+2Na]^+$ in moderate intensity. Cleavage of the N-glycosidic bond to form the sodium cationized cytosine nucleobase $[Cyt+Na]^+$, and deprotonated, disodium cationized cytosine $[Cyt-H+2Na]^+$ was also observed in small abundance. In contrast, photodissociation of $[pCyd-H+2Na]^+$ primarily results in the loss of a water molecule. Pathways involving cleavage of the N-glycosidic bond resulting in $[Cyt+Na]^+$ and $[Cyt-H+2Na]^+$ were observed in small abundance. However, only a minor abundance of $[PO_3+2Na]^+$ and $[H_2PO_4+2Na]^+$ were observed. The IRMPD action spectra of 2′-deoxycytidine ions measured in previous work are compared with that measured for $[pdCyd-H+2Na]^+$ in Fig. 3. Additional comparisons of the experimental IRMPD spectra of cytidine and 2′-deoxycytidine nucleoside and nucleotide ions are shown in Figs. S6 and S7. The IRMPD action spectra measured for the analogous cytidine ions are extremely parallel and thus not shown. The absence of a C=O stretch at ~1790 cm^{-1} in the measured spectra of the sodium cationized ions indicates that a sodium cation must be bound to O2 on the nucleobase in the experiments. The measured IRMPD spectra for $[dCyd+Na]^+$, $[pdCyd+Na]^+$, and $[pdCyd-H+2Na]^+$ are very parallel, suggesting that similar conformations are adopted by the ion populations. The measured IRMPD action spectra of the protonated 2′-deoxycytidine nucleoside $[dCyd+H]^+$ and nucleotide $[pdCyd+H]^+$ are also very similar in peak position, but notably distinct from those of the sodium cationized ions, with a prominent feature at ~1790 cm^{-1} attributed to the nucleobase carbonyl stretch. The measured IRMPD spectrum of deprotonated $[pdCyd-H]^-$ is notably different from those of both the protonated and sodium cationized ions, and lacks the characteristic carbonyl stretch, indicating that O2 is involved in some intramolecular hydrogen-bonding interaction. The hydrogen-stretching region of the measured spectra are all highly parallel in the positions of the major features. However, the similarity observed in the hydrogen-stretching region does not ensure that similar hydrogen-bonding networks must be observed for these ions as there are more available hydrogen-stretching modes in each ion than individual features in the corresponding spectrum. The measured spectra in the IR fingerprint region, especially between 1300−1800 cm^{-1}, do however clearly indicate differences in conformation as a result of the local environment, with sodium cationization, protonation, and deprotonation all clearly differentiable in this region.

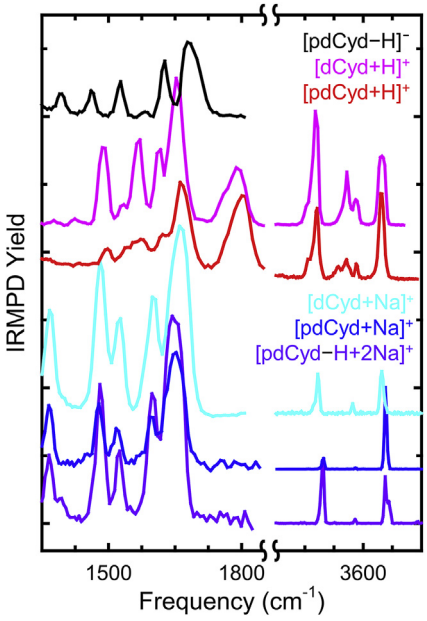

Fig. 3. Comparison of the experimental IRMPD action spectra of the deprotonated, protonated, and sodium cationized quasimolecular ions of 2′-deoxycytidine and 2′-deoxycytidine-5′-monophosphate. IRMPD spectra for $[pdCyd-H]^-$, $[dCyd+H]^+$, $[pdCyd+H]^+$, $[dCyd+Na]^+$, $[pdCyd+Na]^+$, and $[pdCyd-H+2Na]^+$ are taken from Refs. [45,51,66,74,75].

4. Discussion

4.1. Conformers of $[pdCyd-H+2Na]^+$ populated by ESI

Conformers displaying reasonable agreement between their predicted IR spectra and the measured IRMPD spectrum of $[pdCyd-H+2Na]^+$ are shown in Fig. 4 along with their relative Gibbs energies. These four conformers are also excellent examples of the range of conformers that predict IR spectra in reasonable agreement with the major features of the measured IRMPD action spectrum. Structures representing the broader range of stable conformers calculated are shown in Fig. S1, and comparisons of their predicted IR spectra with the measured IMRPD spectrum are provided in Fig. S8. Most of the conformers calculated exhibit reasonable agreement across the IR fingerprint and hydrogen-stretching regions, although some conformers such as $\beta_1\gamma_1 H_{pdC}$, shown in Fig. S8 exhibit more significant disagreement, predicting the wrong peak shape and position at ~1660 cm^{-1}. A consistent feature of the conformers that exhibit the best agreement, such as $\alpha_4\beta_2 A_{pdC}$, $\alpha_1\gamma_2 B_{pdC}$, and $\alpha_1\gamma_1 J_{pdC}$, is a sodium cation bound between an Ox atom and O2. The disagreement shown by $\alpha_1\gamma_1 J_{pdC}$ at ~3520 cm^{-1} is a result of the hydrogen-bound O3′−H stretch and would not be expected to be present as predicted in the measured spectrum due to its anharmonicity. The exact binding of this sodium cation, whether to only Ox and O2, as in $\alpha_1\gamma_1 J_{pdC}$, or with other binding sites on the phosphate, nucleobase, or sugar moieties has relatively little impact on the overall agreement of the predicted IR spectra with the experimental IRMPD spectrum. Several

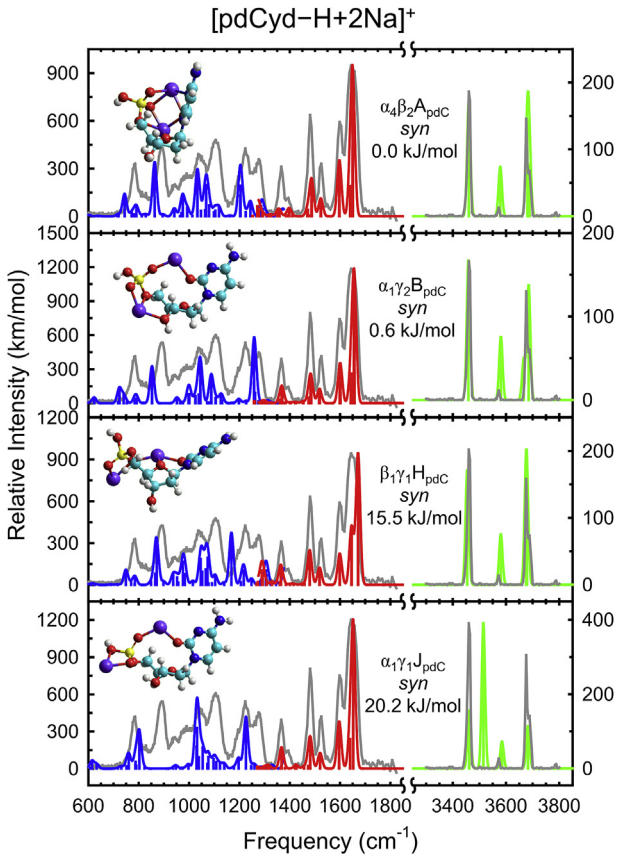

Fig. 4. Comparison of the measured IRMPD action spectrum of $[pdCyd-H+2Na]^+$ with the B3LYP/6-311+G(d,p) predicted linear IR spectra for the representative low-energy conformers populated in the experiments. The sodium cation binding modes, nucleobase orientations, and relative B3LYP/6-311+G(2d,2p) Gibbs energies at 298 K are provided for each conformer. The measured IRMPD yield is shown in gray and normalized to the predicted IR intensities to facilitate visual comparison.

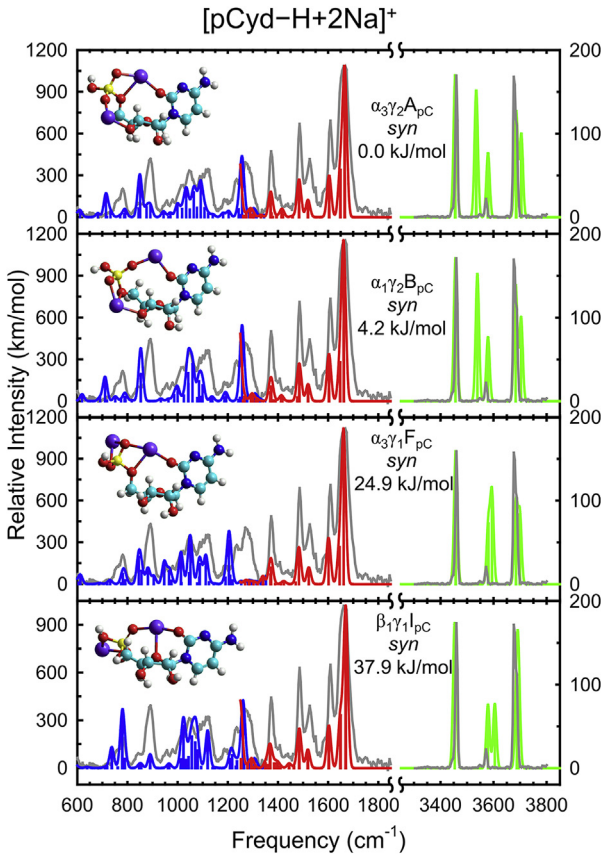

Fig. 5. Comparison of the measured IRMPD action spectrum of $[pCyd-H+2Na]^+$ with the B3LYP/6-311+G(d,p) predicted linear IR spectra for the representative low-energy conformers populated in the experiments. The sodium cation binding modes, nucleobase orientations, and relative B3LYP/6-311+G(2d,2p) Gibbs energies at 298 K are provided for each conformer. The measured IRMPD yield is shown in gray and normalized to the predicted IR intensities to facilitate visual comparison.

binding modes of the second sodium cation are found, with conformers displaying binding to the Ox and OH_p atoms of the phosphate, bridging the phosphate and sugar moiety, and additional binding of the phosphate and nucleobase moieties. The $\alpha_4\beta_2A_{pdC}$, $\alpha_1\gamma_2B_{pdC}$, and $\alpha_1\gamma_1J_{pdC}$ conformers shown in Fig. 4 display the best agreement with the measured spectrum as a group. However, no individual conformer presents the obvious best match, instead it is likely that several more conformers sharing the $Ox\cdots Na^+\cdots O2$ binding mode, core to the α binding modes, are present in the experiments.

4.2. Conformers of $[pCyd-H+2Na]^+$ populated by ESI

The predicted IR spectra of low-energy conformers of $[pCyd-H+2Na]^+$ and displaying reasonable agreement with the measured IRMPD spectrum are compared in Fig. 5. Structures more comprehensively representative of the stable conformers calculated are compared in Fig. S9. As was also observed for $[pdCyd-H+2Na]^+$, most conformers present reasonable agreement across the 1300–1800 cm^{-1} range. However, unlike the DNA analogue, the hydrogen-stretching region of $[pCyd-H+2Na]^+$ exhibits poorer agreement for many conformers primarily with the small feature at ~3570 cm^{-1} and splitting of the feature at ~3680 cm^{-1}, and thus enables better differentiation between the conformers. As found for $[pdCyd-H+2Na]^+$, the α binding modes provide the best overall agreement with the measured IRMPD spectrum of $[pCyd-H+2Na]^+$. The two most stable conformers calculated, which also display the γ_2 binding mode, provide the best overall agreement, but other binding modes such as γ_1 are likely also present in the experiments and contribute to some of the minor features below 1300 cm^{-1}. Similar to $\alpha_1\gamma_1J_{pdC}$, the two most stable conformers predict reasonably intense features at ~3540 cm^{-1} resulting from the hydrogen-bound O3′–H stretch that would not be expected to be observed experimentally.

4.3. Impact of a second sodium cation on structure

As might be expected, every conformer calculated for neutral (pdCyd−H+Na) and (pCyd−H+Na) binds the sodium cation to the deprotonated phosphate moiety. However, conformers that also bind to the nucleobase are certainly preferred, with both (pdCyd−H+Na) and (pCyd−H+Na) preferring the α_3 binding mode between Ox, O2, and O5′. This is consistent with the preference for stabilizing the nucleobase and phosphate moiety of $[pdCyd+Na]^+$ and $[pCyd+Na]^+$ through α binding modes with the Ox and O2 atoms [66]. The presence of a second sodium cation in $[pdCyd-H+2Na]^+$ and $[pCyd-H+2Na]^+$ does not shift this preference much, with α binding modes still generally preferred. However, the binding of a second sodium cation often disrupts the Ox, O2, O5′ interaction preferred by the single sodium cation. The γ_2 binding of a second sodium cation in the low-energy $\alpha_1\gamma_2$ conformers observed for both $[pdCyd-H+2Na]^+$ and $[pCyd-H+2Na]^+$

prioritizes binding to O5′, disrupting the α_3 Ox, O2, O5′ binding preferred by the single sodium cation. Similarly, the β_2 binding mode prioritizes binding to O5′ and prefers an α binding mode involving both Ox atoms and O2 in an α_3 or α_4 binding mode. Although binding of the second sodium cation disrupts the preferred binding mode observed in (pdCyd−H+Na) and (pCyd−H+Na), the core Ox···Na^+···O2 binding is generally retained. In the most stable conformers, the second sodium cation either binds to the nucleobase and phosphate moiety or binds to the phosphate and sugar moieties. Although binding of a second sodium cation can disrupt the specific preferred binding of neutral (pdCyd−H+Na) and (pCyd−H+Na) ion pairs, the overall binding preference remains consistent.

4.4. Impact of the phosphate moiety on neutral cytidine structure

A previous study of the gas-phase conformations of $[pdCyd+Na]^+$ and $[pCyd+Na]^+$ also included theoretical calculations of the conformations of neutral pdCyd and pCyd [66]. The energetically preferred conformers of neutral pdCyd and pCyd both display OH_p···O2 intramolecular hydrogen-bonding interactions. This interaction is a close analogue of the O5′H···O2 hydrogen-bonding interaction observed in the most stable neutral dCyd conformer calculated in previous work [45]. The preferred O5′H···O2 intramolecular hydrogen-bond stabilization of dCyd is maintained in the presence of the phosphate moiety as well; however, the increased flexibility offered by the phosphate moiety does appear to slightly shift the angle of the glycosidic bond. Further, the additional hydrogen-bonding sites on the phosphate also allow for an additional hydrogen-bonding interaction between the phosphate moiety and O3′.

The presence of the 2′-hydroxy moiety in Cyd results in a preference for the O3′H···O2′H···O2 dual hydrogen-bonding interaction over O5′H···O2 hydrogen-bonding. This dual hydrogen-bonding interaction is also observed for pCyd in a conformer found lying just 4.3 kJ/mol above the calculated ground conformer. The opportunity the phosphate moiety provides for an alternative Ox···O3′H···O2′ dual hydrogen-bonding interaction in addition to the O5′H···O2 hydrogen-bonding interaction is likely responsible for the change in the hydrogen-bonding found in the calculated ground conformers of Cyd and pCyd. However, the presence of the 2′-hydroxy moiety in pCyd does have a similar impact on the hydrogen-bonding interactions available to low-energy conformers, with two conformers of pCyd displaying some O2···O2′H hydrogen-bonding interaction, similar to the conformers calculated for Cyd.

4.5. Impact of protonation vs sodium cationization on nucleoside structure

The RMSD analysis described previously [57] was used to select unique conformers of $[dCyd+H]^+$, $[Cyd+H]^+$, $[dCyd+Na]^+$, and $[Cyd+Na]^+$ from those calculated in the previous work of Wu et al. and Zhu et al. with an RMSD cut-off of 10° [45,51]. For these cytidine nucleosides the RMSD cut-off of 10° was used to imitate the manual selection process that took place in the previous studies, but was only partially completed in the calculated conformers readily available for this analysis. The RMSD analysis is also effective in focusing on the most structurally differentiable conformers calculated. A comparison of three conformers of $[dCyd+Na]^+$ is shown in Fig. S3 and demonstrates the utility of the RMSD cut-off at identifying unique conformers. An RMSD of 16.8° was found between the T(O2O5′O4′) and B(O2O5′) conformers, which are quite similar in sodium binding mode, but differ slightly in glycosidic bond angle and sugar puckering. A much larger RMSD of 88.4° was found between T(O2O5′O4′) and B(O2N3), which are more notably different in binding, glycosidic bond angle, sugar pucker, and 5′-hydroxy orientation.

Glycosidic bond angles and the 5′-hydroxy moiety orientations were extracted from the selected unique cytidine nucleoside conformers and plotted in Fig. 6. Protonated conformers with *anti* nucleobase orientations, stabilized by noncanonical C6H···O5′ intramolecular hydrogen-bonding interactions are notably more common in the calculations than those with *syn* nucleobase orientations, and examples of both of these orientations are shown in Fig. 6. Protonated conformers with *syn* nucleobase orientations display intramolecular hydrogen-bonding interactions between O2 and O5′, analogous to the α_1 binding between Ox of the phosphate moiety and O2 of the nucleobase described in this work, and examples of conformers with this hydrogen-bonding interaction are shown for $[dCyd+H]^+$ and $[Cyd+H]^+$ in Fig. 1. The distributions of *anti* and *syn* glycosidic bond angles observed for $[dCyd+H]^+$ and $[Cyd+H]^+$ are generally reproduced upon sodium cationization. However, the prevalence of a specific β_1-like binding, T(O2O5′O4′), with the sodium cation bound above the plane of the sugar moiety

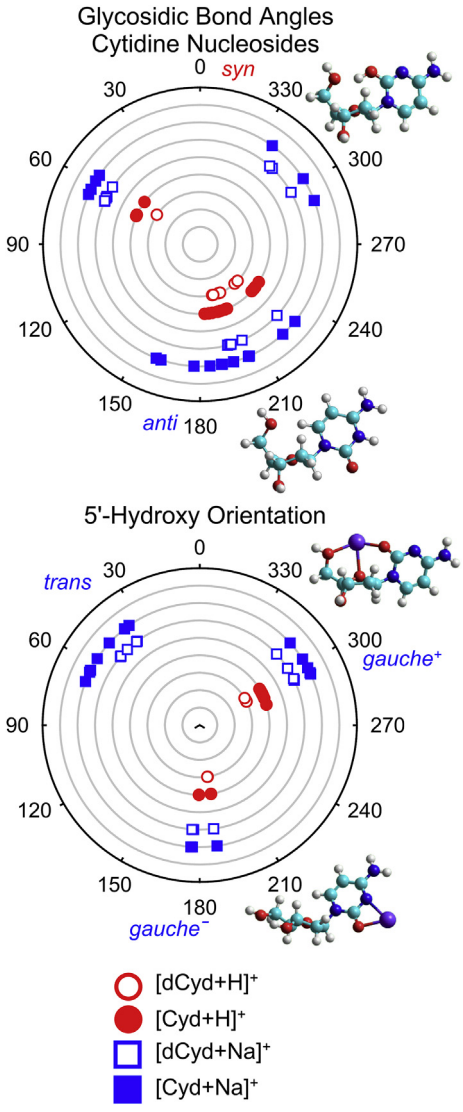

Fig. 6. The glycosidic bond angle of the nucleobase and 5′-hydroxy orientation for the calculated low-energy conformers of the protonated and sodium cationized 2′-deoxycytidine and cytidine nucleosides examined in previous work [45,51].

results in many more conformers with glycosidic bond angles of ~60°. An example of a conformer with T(O2O5′O4′) binding is shown for $[dCyd+Na]^+$ in Fig. 1. Unique to $[dCyd+Na]^+$ and $[Cyd+Na]^+$ are conformers with glycosidic bond angles around ~315°. These conformers are generally also T(O2O5′O4′) β_1-like conformers, but bind the sodium cation behind the ring (see for example the specific β_1 binding conformer shown in Fig. 2). This glycosidic bond angle is also exhibited by conformers that bind the sodium cation between O2 and O2′ in an ε_2-like binding mode, as shown for $[Cyd+Na]^+$ in Fig. 1. Similar conformers are not observed for the protonated cytidine nucleosides as there are no opportunities for hydrogen-bonding with the nucleobase in that orientation and more stable nucleobase orientations are preferred in the absence of hydrogen-bonding interactions with the nucleobase as shown in Fig. 1. The orientations of the 5′-hydroxy moiety in conformers of $[dCyd+H]^+$ and $[Cyd+H]^+$ fall well within the expected ranges for the *gauche*$^+$ and *trans* orientations shown in Fig. 6. No conformers within the Gibbs energy range examined in the previous work for $[dCyd+H]^+$ and $[Cyd+H]^+$ exhibited *gauche*$^-$ 5′-hydroxy moieties. All three 5′-hydroxy orientations are represented within the calculated low-energy conformers of $[dCyd+Na]^+$ and $[Cyd+Na]^+$. The *gauche*$^+$ orientation is often exhibited by the T(O2O5′O4′) binding mode where the sodium cation is bound above the plane of the sugar ring. Conformers with the alternative of the T(O2O5′O4′) binding mode with the sodium cation bound behind the sugar ring exhibit the *gauche*$^-$ orientation. Conformers that display bidentate binding modes that do not involve the 5′-hydroxy substituent display a broader range of orientations, but are solely responsible for conformers with the *trans* 5′-hydroxy moiety orientation.

4.6. Impact of ionization on cytidine monophosphate structure

Several previous IRMPD action spectroscopy studies have examined various quasimolecular forms of the 2′-deoxycytidine and cytidine nucleotides. These forms include the deprotonated anions $[pdCyd-H]^-$ and $[pCyd-H]^-$ [73,74], the protonated cations $[pdCyd+H]^+$ and $[pCyd+H]^+$ [75], and the sodium-bound cations $[pdCyd+Na]^+$ and $[pCyd+Na]^+$ [66]. Both $[pdCyd-H]^-$ and $[pCyd-H]^-$ prefer to stabilize the deprotonated phosphate moiety to the sugar moiety through an Ox···HO3′ hydrogen-bonding interaction as shown in Fig. 1. In $[pCyd-H]^-$, this is extended to an Ox···HO3′···HO2′ hydrogen-bonding interaction. This contrasts with $[pdCyd+H]^+$ and $[pCyd+H]^+$, where the phosphate moiety and nucleobase orientation are stabilized via a noncanonical C6H···Ox hydrogen-bonding interaction. In both the deprotonated and protonated cytidine nucleotides, the primary mode of stabilization involves the phosphate and nucleobase moieties. The binding of the sodium cation allows for a longer interaction distance between the phosphate and nucleobase thus allowing for secondary stabilizing interactions, primarily between the phosphate and sugar moieties. Secondary hydrogen-bonding interactions are available to the deprotonated and protonated cytidine nucleotides as well, but are often competitive with the preferred interactions between the phosphate and nucleobase. For $[pdCyd+Na]^+$ and $[pCyd+Na]^+$, a preference is observed for the tridentate α_2 binding mode between Ox, O2, and N3, with additional hydrogen-bonding interactions between the phosphate and sugar moieties. Additional hydrogen-bonding interactions are less common in the conformers calculated for $[pdCyd-H+2Na]^+$ and $[pCyd-H+2Na]^+$, likely due to the hydrogen-bond acceptors being largely occupied by a sodium cation. The second sodium cation often participates in complex stabilizing interactions of the phosphate, sugar, or nucleobase moieties instead of the hydrogen-bonding that was observed for the deprotonated and protonated nucleotides.

Unique structures were extracted from the conformers calculated in previous studies of the deprotonated, protonated, and sodium cationized DNA and RNA cytidine nucleotides using the RMSD analysis described elsewhere, with a final RMSD cut-off of 10° [66,73–75]. The calculated glycosidic bond angles and O5′ orientations for these unique conformers of $[pdCyd-H]^-$, $[pCyd-H]^-$, $[pdCyd+H]^+$, and $[pCyd+H]^+$ as well as $[pdCyd+Na]^+$, $[pCyd+Na]^+$, $[pdCyd-H+2Na]^+$, and $[pCyd-H+2Na]^+$ are shown in Fig. 7. The protonated and deprotonated cytidine monophosphates all display similar glycosidic bond angle distributions. The protonated or deprotonated forms of the cytidine nucleotides appear to prefer the *anti* nucleobase orientation, stabilized by a C6H···Ox noncanonical hydrogen-bonding interaction. However, some conformers with a *syn* nucleobase orientation are also observed. The range of glycosidic bond angles for $[pdCyd-H]^-$ and $[pCyd-H]^-$ (~180–250°) is broader than that of $[pdCyd+H]^+$ and $[pCyd+H]^+$ (~180–225°), likely due to more conformers with hydrogen-bonding interactions between the phosphate and sugar moieties resulting in a less constrained nucleobase orientation. Also evident in the glycosidic

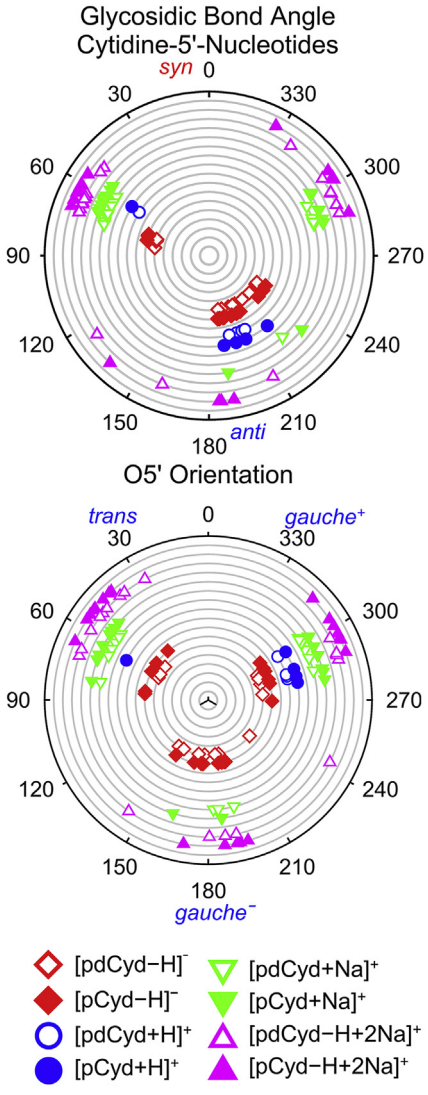

Fig. 7. The glycosidic bond angle of the nucleobase and O5′ dihedral angle for the calculated low-energy conformers of the deprotonated, protonated, and sodium cationized, and deprotonated disodium cationized 2′-deoxycytidine and cytidine-5′-nucleotides [66,73–75].

bond angles shown in Fig. 7 is the impact of sodium cationization vs protonation or deprotonation. The impact of the sodium cation on accessible conformations is highly parallel to that observed for the cytidine nucleosides, as conformers with the β_1 binding mode between Ox, O2, and O4′ typically display glycosidic bond angles of ~310°, which are not exhibited by protonated or deprotonated conformers. The presence of the second sodium cation in $[pdCyd-H+2Na]^+$ and $[pCyd-H+2Na]^+$ does not significantly alter the most common *syn* glycosidic bond angle distributions observed in $[pdCyd+Na]^+$ and $[pCyd+Na]^+$ as the most common sodium binding modes are largely consistent between the systems. A greater difference is observed between the sodium cationized conformers with *anti* nucleobase orientations, but all of these conformers are relatively high in Gibbs energy. Due to the conformers with *anti* nucleobase orientations lying much higher in Gibbs energy, this difference in glycosidic bond angles might also be a result of poor sampling of higher energy conformers between the two sodium cationized cytidine nucleotide systems. The orientations of O5′ are reasonably consistent across the cytidine nucleotide quasimolecular forms examined in Fig. 7. However, none of the protonated cytidine nucleotides display *gauche*$^-$ orientations, which is likely a result of the relatively few higher energy conformers available for this analysis. The distributions of phosphate dihedral angles are shown in Fig. S10. Unlike the glycosidic bond angle and O5′ dihedral angle, the phosphate moiety displays a reasonably continuous distribution around the O5′-C5′ bond, with only the small section of 0°±24° where no phosphate moieties were observed amongst the conformers examined. The local environment of the cytidine nucleotides has some impact on glycosidic bond angle, O5′ orientation, and phosphate moiety orientation. However, the most obvious impact is on glycosidic bond angle where the protonated and deprotonated quasimolecular forms are observed spectroscopically with *anti* nucleobase orientations vs the *syn* nucleobase orientations observed for the sodium cationized nucleotides.

5. Conclusions

Detailed experimental studies of the intrinsic gas-phase conformations of the DNA and RNA cytidine nucleosides and nucleotides by IRMPD and theoretical calculations offers the opportunity to study intrinsic structure as a function of local environment. The increased length and complexity of interactions with a sodium cation vs a proton shifts the glycosidic bond angle distributions of the experimentally populated conformers of the sodium cationized DNA and RNA cytidine nucleosides vs their protonated counterparts. $[dCyd+H]^+$ and $[Cyd+H]^+$ both prefer *anti* nucleobase orientations, primarily stabilized by noncanonical C6H···O5′ hydrogen-bonding interactions. The sodium cationized $[dCyd+Na]^+$ and $[Cyd+Na]^+$ nucleosides energetically prefer *syn* nucleobase orientations in a β_1-like T(O2O5′O4′) binding mode. However, in the previous IRMPD experiments of $[Cyd+Na]^+$, kinetically trapped conformers displaying ε_2-like binding to O2 and O2′ of the nucleobase and sugar moieties were observed experimentally as well. In the presence of the phosphate moiety however, the impact of the sodium cation on the low-energy conformers calculated is more noticeable. This is a result of the increased flexibility of the phosphate moiety vs the 5′-hydroxy substituent and the greater number of binding sites allowing for a wider variety of conformations lying relatively low in Gibbs energy at 298 K. Deprotonation and binding of a second sodium cation in $[pdCyd-H+2Na]^+$ and $[pCyd-H+2Na]^+$ vs $[pdCyd+Na]^+$ and $[pCyd+Na]^+$ does not significantly impact glycosidic bond angles of the low-energy conformations calculated. Binding of a sodium cation between Ox and O2, with additional chelation interactions possible, is preferred for both systems. The spectroscopic results presented in this work indicate that the additional sodium cation in both $[pdCyd-H+2Na]^+$ and $[pCyd-H+2Na]^+$ is preferentially bound to the phosphate and sugar moieties through Ox and O3′ in a γ_2 binding mode, again with potential additional chelation interactions. The specific binding mode preferred between Ox and O2 shifts from the α_2 binding preferred by $[pdCyd+Na]^+$ and $[pCyd+Na]^+$ to α_3 binding, likely to better facilitate the binding of the second sodium cation.

Analysis of calculated conformers from previous studies of the gas-phase quasimolecular forms of the cytidine nucleic acid monomers reveals some notable trends in the glycosidic bond angles of low-energy conformers. The trends observed for the protonated and sodium cationized DNA and RNA nucleosides are similar to those observed for the analogous cytidine nucleotides. The deprotonated and protonated forms of the DNA and RNA cytidine nucleotides exhibit similar distributions of glycosidic bond angles with a notable preference for *anti*-oriented nucleobases stabilized by intramolecular hydrogen-bonding interactions between the phosphate and nucleobase moieties. The distributions of *anti* glycosidic bond angles are also similar between these deprotonated and protonated cytidine nucleotides and the protonated cytidine nucleosides where the intramolecular hydrogen-bonding occurs between the 5′-hydroxy substituent and nucleobase. The binding of a sodium cation by the DNA and RNA cytidine nucleotides strongly prefers the *syn* nucleobase orientation to enable an α binding mode with the sodium cation bound by an Ox atom of the phosphate and the O2 atom of the nucleobase and additional potential chelation interactions. These α binding modes are consistently preferred energetically and spectroscopically when either one or two sodium cations are bound to the nucleotide. The second sodium cation of the disodium cationized deprotonated nucleotides prefers binding between the phosphate and sugar moiety. Several conformations of $[pdCyd-H+2Na]^+$ and $[pCyd-H+2Na]^+$ displaying α and γ binding modes between the phosphate and nucleobase and phosphate and sugar moieties, respectively, are present in these experiments.

Compiling the results of this work with the previous systematic and detailed studies of intrinsic cytidine structure also reveals some insight into the behavior of the cytidine nucleic acid monomers in nucleic acid polymers. Involvement of the phosphate moiety of the phosphate backbone in DNA and RNA will likely prevent the primary α, or even β binding modes between the phosphate and nucleobase described in this work. However, the γ binding modes to the phosphate or between the phosphate and sugar moiety preferred by many of the low-energy conformers in this work indicate that sodium cation binding in DNA and RNA is likely preferred along the backbone. The kinetic trapping of conformers with ε_2-like binding between the nucleobase and sugar moiety observed for $[Cyd+Na]^+$ suggests that sodium binding in the groove may also be available [51]. However, this work demonstrates that the phosphate moiety is the intrinsically preferred site of binding consistent with previous findings.

Funding

Financial support for this work was provided by the National Science Foundation, grant numbers OISE-0730072 and OISE-1357787 (for the FEL IRMPD measurements and international travel), DBI-0922818 (for the Bruker amaZon ETD QITMS) and CHE-1709789 (other research costs). Support from a Thomas C. Rumble Graduate Fellowship is acknowledged by Y.-w. Nei and L.A. Hamlow, with additional support from a Wilfried Heller Research Fellowship and Wayne State University Summer Dissertation Fellowship for Y.-w. Nei.

Declaration of competing interest

The authors declare that they have no known competing financial interests or personal relationships that could have appeared to influence the work reported in this paper.

Acknowledgements

The authors thank Wayne State University Computing & Information Technology for the computational resources and support. The authors are grateful for the financial support of the FELIX laboratory by the Nederlandse Organisatie voor Wetenschappelijk Onderzoek (NWO). The skilled assistance of the FELIX staff is also greatly appreciated.

Appendix A. Supplementary data

Supplementary data to this article can be found online at https://doi.org/10.1016/j.ijms.2019.116234.

References

[1] M. Sundaralingam, Structure and conformation of nucleosides and nucleotides and their analogs as determined by X-ray diffraction, Ann. Ny. Acad. Sci. 255 (1975) 3–42.
[2] M. Sundaralingam, Stereochemistry of nucleic acids and their constituents. IV. Allowed and preferred conformations of nucleosides, nucleoside mono-, di-, tri-, tetraphosphates, nucleic acids and polynucleotides, Biopolymers 7 (1969) 821–860.
[3] S. Arnott, The geometry of nucleic acids, Prog. Biophys. Mol. Biol. 21 (1970) 265–319.
[4] D.B. Davies, S.S. Danyluk, Nuclear magnetic resonance studies of 5′-ribo- and deoxyribonucleotide structures in solution, Biochemistry 13 (1974) 4417–4434.
[5] F.E. Hruska, D.J. Wood, T.N. McCaig, A.A. Smith, A. Holy, A nuclear magnetic resonance study of nucleoside conformation in solution. The effect of structure and conformation on the magnetic nonequivalence of the 5′-methylene hydrogens, Can. J. Chem. 52 (1974) 497–508.
[6] W. Saenger, Principles of Nucleic-Acid Structure, Springer-Verlag, New York, 1984.
[7] S. Arnott, D.W.L. Hukins, Optimised parameters for A-DNA and B-DNA, Biochem. Bioph. Res. Co. 47 (1972) 1504–1509.
[8] T.M. Alam, G.P. Drobny, Solid-state NMR studies of DNA structure and dynamics, Chem. Rev. 91 (1991) 1545–1590.
[9] K. Gehring, J.-L. Leroy, M. Guéron, A tetrameric DNA structure with protonated cytosine-cytosine base pairs, Nature 363 (1993) 561–565.
[10] D.R. Hare, B.R. Reid, Three-dimensional structure of a DNA hairpin in solution: two-dimensional NMR studies and distance geometry calculations on d(CGCGTTTTCGCG), Biochemistry 25 (1986) 5341–5350.
[11] J. Anastassopoulou, Metal-DNA interactions, J. Mol. Struct. 651 (2003) 19–26.
[12] J. Lipfert, S. Doniach, R. Das, D. Herschlag, Understanding nucleic acid-ion interactions, Annu. Rev. Biochem. 83 (2014) 813–841.
[13] K.J. McConnell, D.L. Beveridge, DNA structure: what's in charge? J. Mol. Biol. 304 (2000) 803–820.
[14] N.V. Hud, M. Polak, DNA–cation interactions: the major and minor grooves are flexible ionophores, Curr. Opin. Struct. Biol. 11 (2001) 293–301.
[15] S.B. Howerton, C.C. Sines, D. VanDerveer, L.D. Williams, Locating monovalent cations in the grooves of B-DNA, Biochemistry 40 (2001) 10023–10031.
[16] V. Tereshko, C.J. Wilds, G. Minasov, T.P. Prakash, M.A. Maier, A. Howard, Z. Wawrzak, M. Manoharan, M. Egli, Detection of alkali metal ions in DNA crystals using state-of-the-art X-ray diffraction experiments, Nucleic Acids Res. 29 (2001) 1208–1215.
[17] J. Oomens, B.G. Sartakov, G. Meijer, G. von Helden, Gas-phase infrared multiple photon dissociation spectroscopy of mass-selected molecular ions, Int. J. Mass Spectrom. 254 (2006) 1–19.
[18] L. MacAleese, P. Maitre, Infrared spectroscopy of organometallic ions in the gas phase: from model to real world complexes, Mass Spectrom. Rev. 26 (2007) 583–605.
[19] L. Jašíková, J. Roithová, Infrared multiphoton dissociation spectroscopy with free-electron lasers: on the road from small molecules to biomolecules, Chem. Eur J. 24 (2018) 3374–3390.
[20] T.D. Fridgen, Infrared consequence spectroscopy of gaseous protonated and metal ion cationized complexes, Mass Spectrom. Rev. 28 (2009) 586–607.
[21] C.N. Stedwell, J.F. Galindo, A.E. Roitberg, N.C. Polfer, Structures of biomolecular ions in the gas phase probed by infrared light sources, Annu. Rev. Anal. Chem. 6 (2013) 267–285.
[22] J. Abi-Ghanem, V. Gabelica, Nucleic acid ion structures in the gas phase, Phys. Chem. Chem. Phys. 16 (2014) 21204–21218.
[23] J.K. Martens, J. Grzetic, G. Berden, J. Oomens, Gas-phase conformations of small polyprolines and their fragment ions by IRMPD spectroscopy, Int. J. Mass Spectrom. 377 (2015) 179–187.
[24] J.-Y. Salpin, S. Guillaumont, J. Tortajada, L. MacAleese, J. Lemaire, P. Maitre, Infrared spectra of protonated uracil, thymine and cytosine, ChemPhysChem 8 (2007) 2235–2244.
[25] K.T. Crampton, A.I. Rathur, Y.-w. Nei, G. Berden, J. Oomens, M.T. Rodgers, Protonation preferentially stabilizes minor tautomers of the halouracils: IRMPD action spectroscopy and theoretical studies, J. Am. Soc. Mass Spectrom. 23 (2012) 1469–1478.
[26] K. Rajabi, E.A.L. Gillis, T.D. Fridgen, Structures of alkali metal ion–adenine complexes and hydrated complexes by IRMPD spectroscopy and electronic structure calculations, J. Phys. Chem. A 114 (2010) 3449–3456.
[27] J.M. Bakker, R.K. Sinha, T. Besson, M. Brugnara, P. Tosi, J.-Y. Salpin, P. Maître, Tautomerism of uracil probed via infrared spectroscopy of singly hydrated protonated uracil, J. Phys. Chem. A 112 (2008) 12393–12400.
[28] B. Chiavarino, M.E. Crestoni, S. Fornarini, D. Scuderi, J.-Y. Salpin, Interaction of cisplatin with adenine and guanine: a combined IRMPD, MS/MS, and theoretical study, J. Am. Chem. Soc. 135 (2013) 1445–1455.
[29] B. Yang, R.R. Wu, N.C. Polfer, G. Berden, J. Oomens, M.T. Rodgers, IRMPD action spectroscopy of alkali metal cation–cytosine complexes: effects of alkali metal cation size on gas phase conformation, J. Am. Soc. Mass Spectrom. 24 (2013) 1523–1533.
[30] M. Lesslie, J.T. Lawler, A. Dang, J.A. Korn, D. Bím, V. Steinmetz, P. Maître, F. Tureček, V. Ryzhov, Cytosine radical cations: a gas-ghase study combining IRMPD spectroscopy, UVPD spectroscopy, ion–molecule reactions, and theoretical calculations, ChemPhysChem 18 (2017) 1293–1301.
[31] Y. Nosenko, F. Menges, C. Riehn, G. Niedner-Schatteburg, Investigation by two-color IR dissociation spectroscopy of Hoogsteen-type binding in a metalated nucleobase pair mimic, Phys. Chem. Chem. Phys. 15 (2013) 8171–8178.
[32] E.A.L. Gillis, T.D. Fridgen, The hydrated Li^+–adenine–thymine complex by IRMPD spectroscopy in the N–H/O–H stretching region, Int. J. Mass Spectrom. 297 (2010) 2–8.
[33] A.A. Power, O.Y. Ali, M.B. Burt, T.D. Fridgen, IRMPD spectroscopic and computational study of gas phase $[M(Ura\text{-}H)(Ura)]^+$ and $[M(Ura\text{-}H)(H_2O)_n]^+$ (M=Sr, Ba; n=1, 2) complexes, Int. J. Mass Spectrom. 330–332 (2012) 233–240.
[34] B. Power, V. Haldys, J.-Y. Salpin, T.D. Fridgen, Structures of bare and singly hydrated $[M(Ura\text{-}H)(Ura)]^+$ (M=Mg, Ca, Sr, Ba) complexes in the gas phase by IRMPD spectroscopy in the fingerprint region, Int. J. Mass Spectrom. 378 (2015) 328–335.
[35] B. Power, V. Haldys, J.-Y. Salpin, T.D. Fridgen, Structures of $[M(Ura\text{-}H)(H_2O)_n]^+$ (M = Mg, Ca, Sr, Ba; n = 1–3) complexes in the gas phase by IRMPD spectroscopy and theoretical studies, J. Mass Spectrom. 51 (2016) 236–244.
[36] C.M. Kaczan, A.I. Rathur, R.R. Wu, Y. Chen, C.A. Austin, G. Berden, J. Oomens, M.T. Rodgers, Infrared multiple photon dissociation action spectroscopy of sodium cationized halouracils: effects of sodium cationization and halogenation on gas-phase conformation, Int. J. Mass Spectrom. 378 (2015) 76–85.
[37] B. Power, S. Rowe, T.D. Fridgen, Ammoniated complexes of uracil and transition metal ions: structures of $[M(Ura\text{-}H)(Ura)(NH_3)]^+$ by IRMPD spectroscopy and computational methods (M = Fe, Co, Ni, Cu, Zn, Cd), J. Phys. Chem. B 121 (2017) 58–65.
[38] B. Yang, R.R. Wu, G. Berden, J. Oomens, M.T. Rodgers, Infrared multiple photon dissociation action spectroscopy of proton-bound dimers of cytosine and modified cytosines: effects of modifications on gas-phase conformations, J. Phys. Chem. B 117 (2013) 14191–14201.
[39] K. Rajabi, K. Theel, E.A.L. Gillis, G. Beran, T.D. Fridgen, The structure of the protonated adenine dimer by infrared multiple photon dissociation spectroscopy and electronic structure calculations, J. Phys. Chem. A 113 (2009) 8099–8107.
[40] J. Oomens, A.R. Moehlig, T.H. Morton, Infrared multiple photon dissociation (IRMPD) spectroscopy of the proton-bound dimer of 1-methylcytosine in the gas phase, J. Phys. Chem. Lett. 1 (2010) 2891–2897.
[41] M. Azargun, T.D. Fridgen, Guanine tetrads: an IRMPD spectroscopy, energy resolved SORI-CID, and computational study of $M(9\text{-ethylguanine})_4^+$ (M = Li, Na, K, Rb, Cs) in the gas phase, Phys. Chem. Chem. Phys. 17 (2015) 25778–25785.
[42] J. Gao, G. Berden, M.T. Rodgers, J. Oomens, Interaction of Cu^+ with cytosine and formation of i-motif-like C–M^+–C complexes: alkali versus coinage metals, Phys. Chem. Chem. Phys. 18 (2016) 7269–7277.
[43] R. Cheng, V.E. Rose, B. Power, T.D. Fridgen, Self-assembled uracil complexes containing tautomeric uracils: an IRMPD spectroscopic and computation study of the structures of gaseous $uracil_nCa^{2+}$ (n = 4, 5, or 6) complexes, Phys. Chem. Chem. Phys. 20 (2018) 572–580.
[44] R. Cheng, E. Loire, T.D. Fridgen, Hydrogen bonding in alkali metal cation-bound i-motif-like dimers of 1-methyl cytosine: an IRMPD spectroscopic and computational study, Phys. Chem. Chem. Phys. 21 (2019) 11103–11110.
[45] R.R. Wu, B. Yang, C.E. Frieler, G. Berden, J. Oomens, M.T. Rodgers, N3 and O2 protonated tautomeric conformations of 2′-deoxycytidine and cytidine coexist in the gas phase, J. Phys. Chem. B 119 (2015) 5773–5784.
[46] R.R. Wu, B. Yang, G. Berden, J. Oomens, M.T. Rodgers, Gas-phase conformations and energetics of protonated 2′-deoxyguanosine and guanosine: IRMPD action spectroscopy and theoretical studies, J. Phys. Chem. B 118 (2014) 14774–14784.

[47] R.R. Wu, B. Yang, G. Berden, J. Oomens, M.T. Rodgers, Gas-phase conformations and energetics of protonated 2′-deoxyadenosine and adenosine: IRMPD action spectroscopy and theoretical studies, J. Phys. Chem. B 119 (2015) 2795–2805.

[48] R.R. Wu, B. Yang, C.E. Frieler, G. Berden, J. Oomens, M.T. Rodgers, Diverse mixtures of 2,4-dihydroxy tautomers and O4 protonated conformers of uridine and 2′-deoxyuridine coexist in the gas phase, Phys. Chem. Chem. Phys. 17 (2015) 25978–25988.

[49] R.R. Wu, B. Yang, C.E. Frieler, G. Berden, J. Oomens, M.T. Rodgers, 2,4-Dihydroxy and O2 protonated tautomers of dThd and Thd coexist in the gas phase: methylation alters protonation preferences versus dUrd and Urd, J. Am. Soc. Mass Spectrom. 27 (2016) 410–421.

[50] Y. Zhu, L.A. Hamlow, C.C. He, J.K. Lee, J. Gao, G. Berden, J. Oomens, M.T. Rodgers, Gas-Phase conformations and N-glycosidic bond stabilities of sodium cationized 2'-deoxyguanosine and guanosine: sodium cations preferentially bind to the guanine residue, J. Phys. Chem. B 121 (2017) 4048–4060.

[51] Y. Zhu, L.A. Hamlow, C.C. He, H.A. Roy, N.A. Cunningham, M.U. Munshi, G. Berden, J. Oomens, M.T. Rodgers, Conformations and N-glycosidic bond stabilities of sodium cationized 2′-deoxycytidine and cytidine: solution conformation of $[Cyd+Na]^+$ is preserved upon ESI, Int. J. Mass Spectrom. 429 (2018) 18–27.

[52] Y. Zhu, L.A. Hamlow, C.C. He, S.F. Strobehn, J.K. Lee, J. Gao, G. Berden, J. Oomens, M.T. Rodgers, Influence of sodium cationization versus protonation on the gas-phase conformations and glycosidic bond stabilities of 2′-deoxyadenosine and adenosine, J. Phys. Chem. B 120 (2016) 8892–8904.

[53] Y. Zhu, H.A. Roy, N.A. Cunningham, S.F. Strobehn, J. Gao, M.U. Munshi, G. Berden, J. Oomens, M.T. Rodgers, Effects of sodium cationization *versus* protonation on the conformations and *N*-glycosidic bond stabilities of sodium cationized uridine and 2′-deoxyuridine: solution conformation of $[Urd+Na]^+$ is preserved upon ESI, Phys. Chem. Chem. Phys. 19 (2017) 17637–17652.

[54] Y. Zhu, H.A. Roy, N.A. Cunningham, S.F. Strobehn, J. Gao, M.U. Munshi, G. Berden, J. Oomens, M.T. Rodgers, IRMPD action spectroscopy, ER-CID experiments, and theoretical studies of sodium cationized thymidine and 5-methyluridine: kinetic trapping during the ESI desolvation process preserves the solution structure of $[Thd+Na]^+$, J. Am. Soc. Mass Spectrom. 28 (2017) 2423–2437.

[55] A. Filippi, C. Fraschetti, F. Rondino, S. Piccirillo, V. Steinmetz, L. Guidoni, M. Speranza, Protonated pyrimidine nucleosides probed by IRMPD spectroscopy, Int. J. Mass Spectrom. 354 (2013) 54–61.

[56] L.A. Hamlow, C.C. He, Z.J. Devereaux, H.A. Roy, N.A. Cunningham, E.O. Soley, G. Berden, J. Oomens, M.T. Rodgers, Gas-phase structures of protonated arabino nucleosides, Int. J. Mass Spectrom. 438 (2019) 124–134.

[57] L.A. Hamlow, Z.J. Devereaux, H.A. Roy, N.A. Cunningham, G. Berden, J. Oomens, M.T. Rodgers, Impact of the 2′- and 3′-sugar hydroxyl moieties on gas-phase nucleoside structure, J. Am. Soc. Mass Spectrom. 30 (2019) 832–845.

[58] C.C. He, L.A. Hamlow, Z.J. Devereaux, Y. Zhu, Y.-w. Nei, L. Fan, C.P. McNary, P. Maître, V. Steinmetz, B. Schindler, I. Compagnon, P.B. Armentrout, M.T. Rodgers, Structural and energetic effects of O2′-ribose methylation of protonated purine nucleosides, J. Phys. Chem. B 122 (2018) 9147–9160.

[59] H.U. Ung, K.T. Huynh, J.C. Poutsma, J. Oomens, G. Berden, T.H. Morton, Investigation of proton affinities and gas phase vibrational spectra of protonated nucleosides, deoxynucleosides, and their analogs, Int. J. Mass Spectrom. 378 (2015) 294–302.

[60] Z.J. Devereaux, H.A. Roy, C.C. He, Y. Zhu, N.A. Cunningham, L.A. Hamlow, G. Berden, J. Oomens, M.T. Rodgers, Influence of 2′-fluoro modification on glycosidic bond stabilities and gas-phase ion structures of protonated pyrimidine nucleosides, J. Fluorine Chem. 219 (2019) 10–22.

[61] E.O. Soley, Z.J. Devereaux, L.A. Hamlow, G. Berden, J. Oomens, M.T. Rodgers, IRMPD action spectroscopy, ER-CID experiments, and theoretical approaches investigate intrinsic L-thymidine properties compared to D-thymidine: findings support robust methodology, Int. J. Mass Spectrom. 441 (2019) 32–43.

[62] Z.J. Devereaux, C.C. He, Y. Zhu, H.A. Roy, N.A. Cunningham, L.A. Hamlow, G. Berden, J. Oomens, M.T. Rodgers, Structures and relative glycosidic bond stabilities of protonated 2′-fluoro-substituted purine nucleosides, J. Am. Soc. Mass Spectrom. 30 (2019) 1521–1536.

[63] Z.A. Tehrani, A. Fattahi, A. Pourjavadi, DFT study of the interaction of cytidine and 2'-deoxycytidine with Li^+, Na^+, and K^+: effects of metal cationization on sugar puckering and stability of the N-glycosidic bond, Carbohydr. Res. 344 (2009) 771–778.

[64] J.-Y. Salpin, L. Gamiette, J. Tortajada, T. Besson, P. Maître, Structure of Pb^{2+}/dCMP and Pb^{2+}/CMP complexes as characterized by tandem mass spectrometry and IRMPD spectroscopy, Int. J. Mass Spectrom. 304 (2011) 154–164.

[65] J.-Y. Salpin, L. MacAleese, F. Chirot, P. Dugourd, Structure of the Pb^{2+}–deprotonated dGMP complex in the gas phase: a combined MS-MS/IRMPD spectroscopy/ion mobility study, Phys. Chem. Chem. Phys. 16 (2014) 14127–14138.

[66] L.A. Hamlow, Y.-w. Nei, R.R. Wu, J. Gao, J.D. Steill, G. Berden, J. Oomens, M.T. Rodgers, Impact of sodium cationization on gas-phase conformations of DNA and RNA cytidine mononucleotides, J. Am. Soc. Mass Spectrom. 30 (2019) 1758–1767.

[67] B. Chiavarino, M.E. Crestoni, S. Fornarini, F. Lanucara, J. Lemaire, P. Maitre, D. Scuderi, Infrared spectroscopy of isolated nucleotides. 1. The cyclic 3′,5′-adenosine monophosphate anion, Int. J. Mass Spectrom. 270 (2008) 111–117.

[68] B. Chiavarino, M.E. Crestoni, S. Fornarini, D. Scuderi, J.-Y. Salpin, Interaction of cisplatin with 5′-dGMP: a combined IRMPD and theoretical study, Inorg. Chem. 54 (2015) 3513–3522.

[69] B. Chiavarino, M.E. Crestoni, S. Fornarini, D. Scuderi, J.-Y. Salpin, Undervalued N3 coordination revealed in the cisplatin complex with 2′-deoxyadenosine-5′-monophosphate by a combined IRMPD and theoretical study, Inorg. Chem. 56 (2017) 8793–8801.

[70] A. Ciavardini, A. Dalla Cort, S. Fornarini, D. Scuderi, A. Giardini, G. Forte, E. Bodo, S. Piccirillo, Adenosine monophosphate recognition by zinc–salophen complexes: IRMPD spectroscopy and quantum modeling study, J. Mol. Spectrosc. 335 (2017) 108–116.

[71] F. Lanucara, M.E. Crestoni, B. Chiavarino, S. Fornarini, O. Hernandez, D. Scuderi, P. Maitre, Infrared spectroscopy of nucleotides in the gas phase 2. The protonated cyclic 3′,5′-adenosine monophosphate, RSC Adv. 3 (2013) 12711–12720.

[72] R.E. van Outersterp, J. Martens, G. Berden, J.D. Steill, J. Oomens, A.M. Rijs, Structural characterization of nucleotide 5′-triphosphates by infrared ion spectroscopy and theoretical studies, Phys. Chem. Chem. Phys. 20 (2018) 28319–28330.

[73] Y.-w. Nei, K.T. Crampton, G. Berden, J. Oomens, M.T. Rodgers, Infrared multiple photon dissociation action spectroscopy of deprotonated RNA mononucleotides: gas-phase conformations and energetics, J. Phys. Chem. A 117 (2013) 10634–10649.

[74] Y.-w. Nei, N. Hallowita, J.D. Steill, J. Oomens, M.T. Rodgers, Infrared multiple photon dissociation action spectroscopy of deprotonated DNA mononucleotides: gas-phase conformations and energetics, J. Phys. Chem. A 117 (2013) 1319–1335.

[75] R.R. Wu, L.A. Hamlow, C.C. He, Y.-w. Nei, G. Berden, J. Oomens, M.T. Rodgers, N3 and O2 protonated conformers of the cytosine mononucleotides coexist in the gas phase, J. Am. Soc. Mass Spectrom. 28 (2017) 1638–1646.

[76] L.A. Hamlow, Y. Zhu, Z.J. Devereaux, N.A. Cunningham, G. Berden, J. Oomens, M.T. Rodgers, Modified quadrupole ion trap mass spectrometer for infrared ion spectroscopy: application to protonated thiated uridines, J. Am. Soc. Mass Spectrom. 29 (2018) 2125–2137.

[77] J. Martens, G. Berden, C.R. Gebhardt, J. Oomens, Infrared ion spectroscopy in a modified quadrupole ion trap mass spectrometer at the FELIX free electron laser laboratory, Rev. Sci. Instrum. 87 (2016), 103108-103108.

[78] K. Wolinski, J.F. Hinton, D.S.S. Wishart, B. D, F.M.P. Richards, A. Saudek, V., P.D. Ellis, G.E. Maciel, J.W.B. McIver Jr., A.C. Santry, D. P, J.A. Pople, N.S.D. Ostlund, L.,J. Hoarau, M.K. Pesquer, M.,I. Ando, R. Chujo, A.V. Nishioka, E.C. Odiot, S.,F. Tonnard, J.D. Baker, M.C.B. Zerner, D. V, W.P.C. Anderson, T.R. Bingham, R.C. Dewar, M.J. S, D.H. Lo, J. Li, P.C. Mello, K. Jug, W. Thiel, E.G.H. Zoebisch, E. F, J. Stewart, M.H.J. P, D.M. Fraser, HyperChem Computational Chemistry Software Package, Version 8.0, Hypercube Inc., Gainesville, FL, 2004.

[79] C. Altona, M. Sundaralingam, Conformational-analysis of sugar ring in nucleosides and nucleotides: new description using concept of pseudorotation, J. Am. Chem. Soc. 94 (1972) 8205–8212.

[80] M.J. Frisch, G.W. Trucks, H.B. Schlegel, G.E. Scuseria, M.A. Robb, J.R. Cheeseman, G. Scalmani, V. Barone, B. Mennucci, G.A. Petersson, H. Nakatsuji, M. Caricato, X. Li, H.P. Hratchian, A.F. Izmaylov, J. Bloino, G. Zheng, J.L. Sonnenberg, M. Hada, M. Ehara, K. Toyota, R. Fukuda, J. Hasegawa, M. Ishida, T. Nakajima, Y. Honda, O. Kitao, H. Nakai, T. Vreven, J.A. Montgomery Jr., J.E. Peralta, F. Ogliaro, M.J. Bearpark, J. Heyd, E.N. Brothers, K.N. Kudin, V.N. Staroverov, R. Kobayashi, J. Normand, K. Raghavachari, A.P. Rendell, J.C. Burant, S.S. Iyengar, J. Tomasi, M. Cossi, N. Rega, N.J. Millam, M. Klene, J.E. Knox, J.B. Cross, V. Bakken, C. Adamo, J. Jaramillo, R. Gomperts, R.E. Stratmann, O. Yazyev, A.J. Austin, R. Cammi, C. Pomelli, J.W. Ochterski, R.L. Martin, K. Morokuma, V.G. Zakrzewski, G.A. Voth, P. Salvador, J.J. Dannenberg, S. Dapprich, A.D. Daniels, Ö. Farkas, J.B. Foresman, J.V. Ortiz, J. Cioslowski, D.J. Fox, Gaussian 09, Gaussian, Inc., Wallingford, CT, 2009.

[81] R.R. Wu, C.C. He, L.A. Hamlow, Y.-w. Nei, G. Berden, J. Oomens, M.T. Rodgers, Protonation induces base rotation of purine nucleotides pdGuo and pGuo, Phys. Chem. Chem. Phys. 18 (2016) 15081–15090.

[82] R.R. Wu, L.A. Hamlow, C.C. He, Y.-w. Nei, G. Berden, J. Oomens, M.T. Rodgers, The intrinsic basicity of the phosphate backbone exceeds that of uracil and thymine residues: protonation of the phosphate moiety is preferred over the nucleobase for pdThd and pUrd, Phys. Chem. Chem. Phys. 19 (2017) 30351–30361.

[83] R.R. Wu, C.C. He, L.A. Hamlow, Y.-w. Nei, G. Berden, J. Oomens, M.T. Rodgers, N3 protonation induces base rotation of 2′-deoxyadenosine-5′-monophosphate and adenosine-5′-monophosphate, J. Phys. Chem. B 120 (2016) 4616–4624.

[84] R.R. Wu, M.T. Rodgers, Mechanisms and energetics for N-glycosidic bond cleavage of protonated adenine nucleosides: N3 protonation induces base rotation and enhances N-glycosidic bond stability, Phys. Chem. Chem. Phys. 18 (2016) 16021–16032.

[85] R.R. Wu, M.T. Rodgers, Tautomerization lowers the activation barriers for N-glycosidic bond cleavage of protonated uridine and 2′-deoxyuridine, Phys.

Chem. Chem. Phys. 18 (2016) 24451–24459.
[86] R.R. Wu, M.T. Rodgers, O2 protonation controls threshold behavior for N-glycosidic bond cleavage of protonated cytosine nucleosides, J. Phys. Chem. B 120 (2016) 4803–4811.
[87] P. Parneix, M. Basire, F. Calvo, Accurate modeling of infrared multiple photon dissociation spectra: the dynamical role of anharmonicities, J. Phys. Chem. A 117 (2013) 3954–3959.
[88] A.P. Scott, L. Radom, Harmonic vibrational frequencies: an evaluation of Hartree–Fock, Møller–Plesset, quadratic configuration interaction, density functional theory, and semiempirical scale factors, J. Phys. Chem. 100 (1996) 16502–16513.